RSC Advances

PAPER

View Article Online
View Journal | View Issue

Cite this: *RSC Adv.*, 2024, **14**, 29368

Porphyrin photosensitizer molecules as effective medicine candidates for photodynamic therapy: electronic structure information aided design†

Wei-Huang Yin,[a] Peng-Yuan Li,[b] Hou-Hou Huang,[b] Lu Feng,[b] Shu-Hui Liu,[b] Xin Liu*[a] and Fu-Quan Bai *[b]

Traditional photosensitizers (PS) in photodynamic therapy (PDT) have restricted tissue penetrability of light and a lack of selectivity for tumor cells, which diminishes the efficiency of PDT. Our aim is to effectively screen porphyrin-based PS medication through computational simulations of large-scale design and screening of PDT candidates *via* a precise description of the state of the light-stimulated PS molecule. Perylene-diimide (PDI) shows an absorption band in the near-infrared region (NIR) and a great photostability. Meanwhile, the insertion of metal can enhance tumor targeting. Therefore, on the basis of the original porphyrin PS segments, a series of metalloporphyrin combined with PDI and additional allosteric Zn-porphyrin-PDI systems were designed and investigated. Geometrical structures, frontier molecular orbitals, ultraviolet-visible (UV-vis) absorption spectra, adiabatic electron affinities (AEA), especially the triplet excited states and spin–orbit coupling matrix elements (SOCME) of these expanded D–A porphyrin were studied in detail using the density functional theory (DFT) and time-dependent density functional theory (TDDFT) methods. PS candidates, conforming type I or II mechanism for PDT, have been researched carefully by molecular docking which targeted Factor-related apoptosis (Fas)/Fas ligand (Fasl) mediated signaling pathway. It was found that porphyrin-PDI, Fe^{2}-porphyrin-PDI, Zn-porphyrin-PDI, Mg-porphyrin-PDI, Zn-porphyrin combined with PDI through single bond (compound **1**), and two acetylenic bonds (compound **2**) in this work would be proposed as potential PS candidates for PDT process. This study was expected to provide PS candidates for the development of novel medicines in PDT.

Received 1st August 2024
Accepted 10th September 2024

DOI: 10.1039/d4ra05585c

rsc.li/rsc-advances

1 Introduction

Cancer remains one of the leading causes of death worldwide, despite the notable efficacy of traditional anticancer modalities, such as surgery and chemoradiotherapy.[1] However, photodynamic therapy (PDT), an alternative to contemporary cancer treatment, has emerged as a successful and clinically approved therapeutic modality.[2] PDT provides several therapeutic preponderances, including selectivity, non-invasiveness, high cure rates and low side effects for the neoplastic management and non-malignant diseases.[3]

PDT is based on the generation of reactive oxygen species (ROS) in order to bring about the induction of death in cancerous tissues.[4] The PDT process involves photosensitizers (PS), molecular oxygen, and light source.[5] Mechanistically, the effect occurs when appropriate energy is absorbed optically by PS, transiting from ground state (S_0) to the first singlet excited state (S_1). After that, the excited triplet state (T_1) is formed through Inter System Crossing (ISC). Subsequently, the T_1 of PS participates in the type I electron transfer reactions to produce ROS. In the type II pathway, the PS transfers energy to triplet molecular oxygen ($^3O_2$), generating highly singlet oxygen ($^1O_2$).[6,7] The production of molecular oxygen, as mentioned above in tissues and cells, initiates three main cell death models: apoptotic, necrotic, and autophagic.[8–10] Significantly, Fas/Fasl mediated signaling pathway is one of the most important apoptosis-related signaling pathways.[11] The abnormal expression of Fas/Fasl was found in the majority cancers, including head and neck squamous cell carcinoma.[12]

At present, PDT is mainly exploited in the treatment of superficial diseases, such as premalignant conditions, carcinoma *in situ* or superficial tumors.[13] However, traditional PS in PDT has a limited excitation wavelength at the phototherapy window (620–850 nm), and other wavelengths of visible light can also damage healthy tissues.[14] Meanwhile, the production of ROS is slashed by the hypoxic environment in the tumor.[15] Therefore, improving the photoelectric conversion efficiency of

[a]*Department of Stomatology, China-Japan Union Hospital of Jilin University, Changchun, Jilin 130033, P. R. China. E-mail: liuxin99@jlu.edu.cn*

[b]*Institute of Theoretical Chemistry and College of Chemistry, Jilin University, Changchun 130023, P. R. China. E-mail: baifq@jlu.edu.cn*

† Electronic supplementary information (ESI) available. See DOI: https://doi.org/10.1039/d4ra05585c

the phototherapy window (focusing on the milder and safer wavelength of 700–850 nm) and enhancing the capacity of oxygen excitation and production are the critical measures to heighten the efficacy of PDT.

The porphyrin segment is the most prominent variety of PS in clinical trials, which is widely present in hemoglobin (iron porphyrin), hemocyanin (copper porphyrin) in animals, chlorophyll (magnesium porphyrin), and cobalt porphyrin in plants.[16] Porphyrin compounds are a class of organic macrocyclic molecules with highly π-conjugated structure, with rich structural diversity and excellent photoelectric properties.[17] The structure of the porphyrin molecule enables straightforward modification by substituting hydrogen atoms at the 8 β positions and the 4 meso-sites with various metal ions, substituents, or conjugated systems.[18] This tunability not only facilitates synthesis and modification but also enables the optimization of their electronic and photophysical properties. As a result, various porphyrin derivatives can be produced, enhancing photosensitizing capabilities while maintaining lower toxicity and improved controllability. Paradoxically, the inadequate selectivity to neoplastic tissues, and weak absorption in the near-infrared region (NIR) of porphyrin compounds limited their further applications in clinical settings.[19] Studies have shown that metalloporphyrin has a good affinity for neoplastic tissues and could selectively stay in cancer cells.[20,21] Additionally, the organic chromophores were introduced into metal complexes can improve the triplet excited state lifetime.[22] Perylene diimide (PDI), a super planar-conjugated system with a special energy level structure, exhibits excellent photochemical properties and tissue penetration in NIR compared to visible light.[23–26] PDI is highly preferred in the field of organic solar cell research, due to its ability to be conjugated with porphyrins, allowing for adjustments in absorption, energy levels, and photovoltaic performance.[27,28] This suggests that the porphyrin-PDI conjugate, forming the Donor–Acceptor (D–A) structure, holds significant promise and has the potential to enhance absorption in the near-infrared (NIR) region.[29]

Herein, a series of porphyrin-based derivatives in group 1 without or with metals (Fe, Zn and Mg) were designed (Scheme 1a), and the D–A metalloporphyrin complexes in group 2 were then constructed with PDI using a push–pull strategy (Scheme 1b). Density functional theory (DFT) is the most effective method to study the electronic structure of their excited states.[30] During the triplet state calculation, it needs to be emphasized that among these design PS, multi-spin states are considered for Fe-porphyrin and Fe-porphyrin-PDI.[31] Therefore, all calculation contents were performed in singlet and quintet states of Fe to discuss in detail.

In brief, the aim of this study is to obtain structural information and photophysical property prediction of all designed porphyrin derivatives more quickly through theoretical simulation. Different from molecular dynamics methods for studying some medicine candidates, PDT requires a more rigorous description of its excited state electronic structure, so that its photoexcited pharmacology can be elaborated. In addition, molecular docking analysis of the PS candidates against cancer-related targeted proteins was also performed.

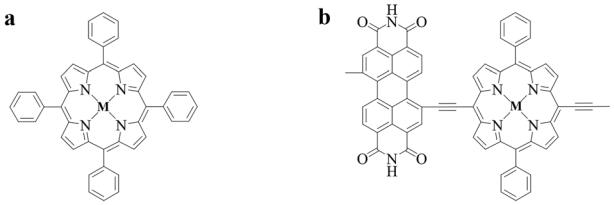

Scheme 1 Molecular structures of (a) M-porphyrin and (b) M-porphyrin-PDI. Fe^1: singlet state; Fe^2: quintet state.

Ultimately, effective porphyrin-based PS were screened as potential candidates for PDT. This study provides valuable information and theoretical foundation for the design and screening of porphyrin-based PS medicine.

2 Method

2.1 DFT calculations

The geometries of the ground state and excited states of all systems were optimized using the density functional theory (DFT) and time-dependent density functional theory (TDDFT) methods respectively. After literature analysis and functional testing, The M06 exchange and correlation functional was selected in this work for electronic structure and electron excited transition calculation.[32,33] The 6-31G (d) basis set was used for C, N, H and O atoms.[34] The LanL2DZ basis set was used for Fe, Zn and Mg.[35] The implicit solvent model PCM was used to simulate the water solvent environment.[36] All geometries reached the minimum point on the potential energy surfaces, which was confirmed through frequency analysis. All computations were performed without symmetry constraints. The above quantum chemical calculations were performed using with Gaussian16 program package.[37]

Spin–orbit coupling (SOC) was calculated through the m06 and ωb97xd method (Fe^1-porphyrin and Fe^2-porphyrin),[38] which was coupled with the def2-TZVP basis set by Orca with TD-DFT.[39] The spin–orbit couplings are defined according to the formula:

$$\mathrm{SOC}_{ij} = \sqrt{\sum_{n} \left|\Psi_{\mathrm{S}_i}\left|\hat{H}_{\mathrm{SO}}\right|\Psi_{\mathrm{T}_j,n}\right|^2} \quad ;\ n = x,\ y,\ z \qquad (1)$$

where $\hat{H}_{\mathrm{SO}}$ represents the spin–orbit Hamiltonian. Ψ_{S_i} and Ψ_{T_j} stand for the wave function of ground state and triplet state, respectively.

2.2 Molecular docking

AutoDock Tools (ADT) was used for docking study.[40] The three-dimensional (3D) structures of proteins were obtained from the RCSB Protein Data Bank (PDB) such as Fas [PDB ID: 1DDF] and Fasl [PDB ID: 5L19]. PDBQT files for protein and ligands preparation and grid box creation, were completed using the graphical user interface program Autodock 4.2.6. Visualization of docking results was performed by using Pymol.[41] The binding free energy of complex (ΔG_{bind}) calculated by ADT was the

difference between the free energies of the complex ($\Delta G_{complex}$) and the unbound receptor (ΔG_{rec}) and the free ligand (ΔG_{lig}) as described by the following equations:

$$\Delta G_{bind} = \Delta G_{complex} - \Delta G_{receptor} - \Delta G_{ligand} \quad (2)$$

3 Result and discussion

PDT has been considered as a clinical option for the treatment of solid tumors. It relies on the ingested PS, following a certain time interval, which is activated by light with a specific wavelength.[42] The mechanism of PDT enforces the following key requirements of effective PS: (1) the capacity to absorb light to the first singlet excited state in the therapeutic window while oscillator strength lager than 0.01; (2) the T_1–S_0 energy gap larger than 0.98 eV, which is the amount of energy required to activate molecular oxygen; (3) the electron affinity of molecular oxygen should be higher than that of PS for obtaining the electron from PS; (4) the SOC values higher than 0.24 cm^{-1} that ensure an efficient ISC process.[43–45]

3.1 Molecular geometries and electronic structures

The geometrically optimized structures of the porphyrin derivatives were shown in Fig. 1a and b. All molecules consist of a porphyrin structure in the center, surrounded by four benzene rings, except for PDI. The porphyrin in the center forms a large conjugated system with a planar structure, while the four surrounding benzene rings maintain a certain dihedral angles to the porphyrin structure, and the values of these dihedral angles were listed in Table 1. A diagram of Fe^1 was presented in Fig. 1c.

For the porphyrin molecule, the values of the four dihedral angles were 62.29°, 62.62°, 62.27°, and 62.62°. Compared to porphyrin, the dihedral angle between the benzene ring and the porphyrin was slightly increased in Fe^1-porphyrin, while it remains essentially unchanged in Fe^2-porphyrin, Zn-porphyrin and Mg-porphyrin. Table 1 also lists the bond lengths of the different metal atoms with the four N atoms. In Zn-porphyrin, the length of the four N–Zn bond was essentially equal, all of which were 2.065 Å. The same was true for the N–Mg bond length of Mg-porphyrin and the N–Fe bond length of Fe^1-porphyrin, which are 2.064 Å and 1.996 Å, respectively. The N–Fe bond length was slightly shorter than N–Zn and N–Mg. In Fe^2-porphyrin, the two N–Fe bond lengths of 2.071 Å for B1 and B3 and 2.048 Å for B2 and B4 were significantly different from the other three molecules.

The obtained vertical excitation energies, excitation wavelengths, oscillator strengths, and the contributions of orbital transitions to electron excitation were reported in Table 2. Frontier molecular orbitals for all complexes were shown in Fig. 2. Frontier molecular orbitals are important for describing the stability using

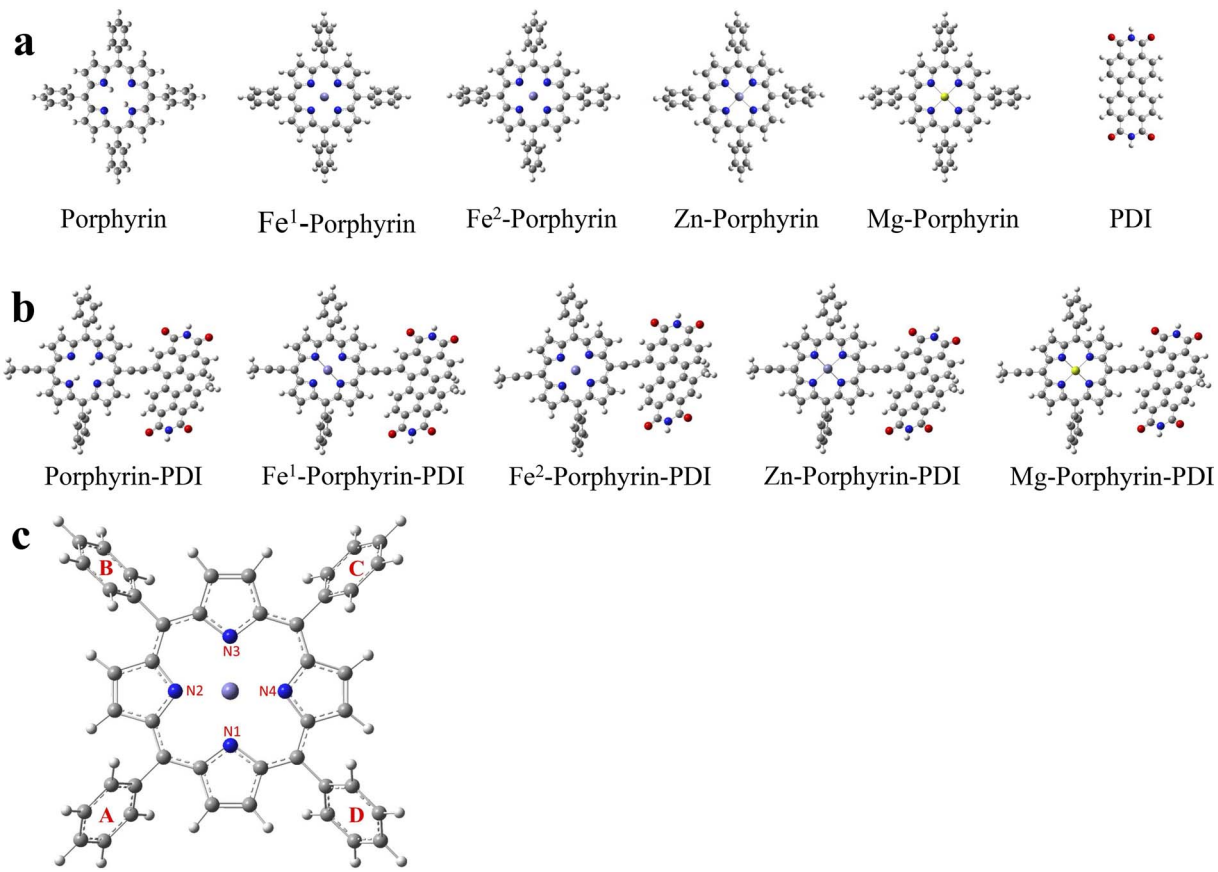

Fig. 1 Optimized ground-state structure of (a) M-porphyrin and (b) M-porphyrin-PDI. (c) The rotation of four benzene rings to porphyrin and the length of metal atoms to N atoms. Fe^1: singlet state; Fe^2: quintet state.

Table 1 The dihedral angles (deg) between the porphyrin and the four benzene rings (A, B, C and D) and the bond lengths (Å) of the different metal atoms to the four N atoms (N1, N2, N3 and N4)

	Porphyrin	Fe^1-porphyrin	Fe^2-porphyrin	Zn-porphyrin	Mg-porphyrin
Dihedral angles					
A-porphyrin	62.293	65.011	62.947	62.840	62.146
B-porphyrin	62.618	64.999	62.363	62.701	61.965
C-porphyrin	62.273	64.829	62.944	62.941	62.125
D-porphyrin	62.625	64.998	62.365	62.843	61.965
Bond lengths					
N1–M	—	1.996	2.071	2.065	2.064
N2–M	—	1.996	2.048	2.065	2.064
N3–M	—	1.996	2.071	2.065	2.064
N4–M	—	1.996	2.048	2.065	2.064

Table 2 The essential vertical excitations of M-porphyrin and M-porphyrin-PDI

	Excitation energy (eV)	Wavelength (nm)	f	Main configuration
Porphyrin	2.1715	570.97	0.0134	H → L (62%)
Fe^1-porphyrin	2.3314	531.81	0.0224	H → L+1 (57%)
Fe^2-porphyrin	2.0054	618.24	0.0106	H → L+1 (71%)
Zn-porphyrin	2.1945	564.98	0.0501	H → L (64%)
Mg-porphyrin	2.1735	570.43	0.0540	H → L (64%)
PDI	2.3958	517.50	0.7816	H → L (100%)
Porphyrin-PDI	1.6992	729.67	0.4667	H → L (96%)
Fe^1-porphyrin-PDI	1.6944	731.74	0.3899	H → L (98%)
Fe^2-porphyrin-PDI	1.1181	742.33	0.3941	H → L (77%)
Zn-porphyrin-PDI	1.6134	768.47	0.3495	H → L (98%)
Mg-porphyrin-PDI	1.5854	782.05	0.3578	H → L (98%)

the LUMO–HOMO gap parameter.[46] Among the porphyrin derivatives, the HOMO, LUMO, and LUMO+1 of all molecules was delocalized on the porphyrin structure, except for the LUMO orbital of Fe^1-porphyrin, which was centrally distributed on the Fe atom. In porphyrin-PDI, Zn-porphyrin-PDI, and Mg-porphyrin-PDI complexes, the HOMO was delocalized on the porphyrin structure while the LUMO was delocalized on the PDI structure. In Fe^1-porphyrin-PDI and Fe^2-porphyrin-PDI, the HOMO is delocalized over the porphyrin segment. Notably, the LUMO in Fe^2-porphyrin-PDI is localized exclusively on the PDI, whereas in Fe^1-porphyrin-PDI, it is distributed over both the porphyrin and the PDI. The stronger orbital coupling between Fe^1-porphyrin and PDI facilitates LUMO delocalization across both regions. In contrast, the weaker coupling in Fe^2-porphyrin-PDI results in the LUMO being primarily confined to the PDI. This difference highlights the impact of spin states on the orbital energy and distribution within the system. Additionally, after incorporating PDI, we observed that the composition of the HOMO−1 remained largely unchanged compared to the standalone metal-porphyrin. However, the LUMO+1 orbital showed greater delocalization across both Fe^1-porphyrin and PDI, indicating stronger interactions between Fe^1 and the ligands. This suggests that the inclusion of PDI enhances electronic transfer between Fe^1 and the surrounding ligands, potentially increasing the efficiency of ISC. Therefore, the PS could realize intramolecular electron transfer upon excited, further demonstrating its D–A structural feature. Since a smaller gap value implied electron easily to transit, our results (Fig. 3) suggested that the gap value of group 2 were smaller than group 1 (0.80, 0.74, 0.86, 0.93, 0.94 eV). It implied that the addition of PDI could reduce the HOMO–LUMO gap.

3.2 Absorption spectra

The wavelength chosen for PDT is typically coincides with the longest-wavelength absorption band of the PS, ideally occurring between 620 and 850 nm.[15] The classic UV-vis absorption spectra of porphyrin compounds can be divided into two characteristic absorption bands: a strong Soret band (350–450 nm) and several weak Q bands (500–650 nm).[20] If some groups were introduced into the porphyrin substrates, the absorption wavelength and the number of peaks in the Q band would be changed.[16] This was due to the symmetry of the porphyrins, variations in the conjugated system, and the degree of distortion.[47] In our study on absorption spectra, group 1 (Fig. 4a) showed typical absorption characteristic of metalloporphyrin in the UV-vis region. However, the addition of metal did not produce a noticeable red-shift effect on the results. In Table 2, their maximum absorption wavelengths were mainly approximately 400 nm, and the absorption within the range of 500 to 650 nm was extremely weak, with an oscillator strength of less than 0.1. In the range of 500–650 nm, for all porphyrin derivatives, the largest contribution to the electronic excitation of all porphyrin derivatives was the HOMO → LUMO transition, except

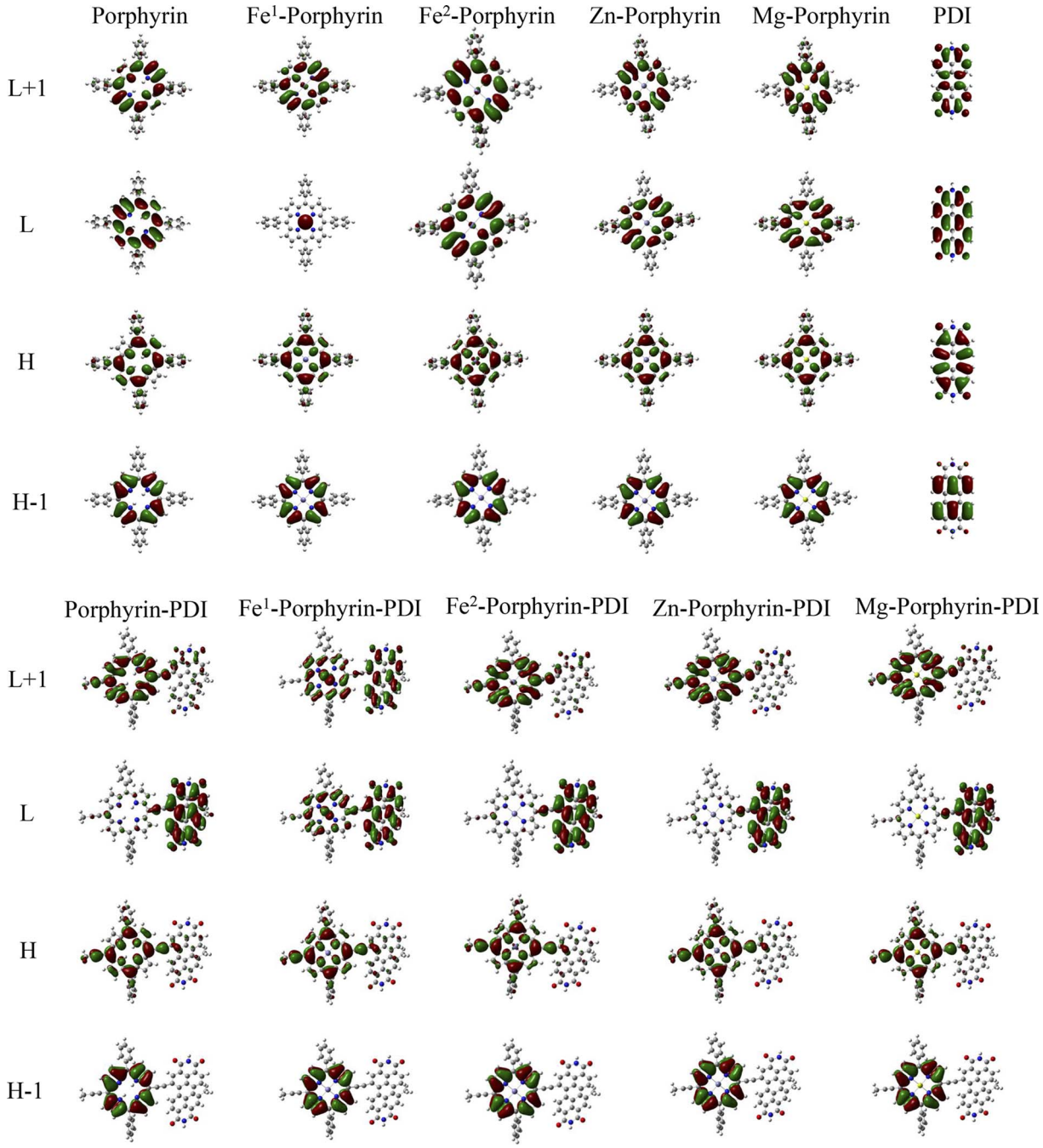

Fig. 2 Graphical representation of the molecular orbitals of M-porphyrin and M-porphyrin-PDI.

for Fe^1/Fe^2-porphyrin, which was a HOMO → LUMO+1 transition, and the electronic excitations of all the molecules were localized excitations on the porphyrin structure. In contrast, in porphyrin-PDI complexes, the HOMO–LUMO transitions involve charge transfer processes from porphyrin to PDI or from PDI to porphyrin, resulting in an appearance of the new absorption band at 700–800 nm and a large oscillator strength. The value of group 2 was sufficient in phototherapy window (Fig. 4b). With the insertion of PDI, it generated a "push–pull" structure with a bigger conjugated system. New peaks appeared in the spectra due to the extended charge transfer transition state, which were located in the NIR. The significant advantage of these compounds lies in their capability to absorb at substantially longer wavelengths (700–850 nm) compared to commonly used porphyrins such as Foscan® (652 nm). Group 2 were chosen to discuss in the following study. Their absorption wavelength occurred in 700–850 nm which would have a deeper tissue penetrability.

3.3 Electron affinity

Electron Affinity (EA) included the vertical electron affinities (VEA) and adiabatic electron affinities (AEA). Considering the

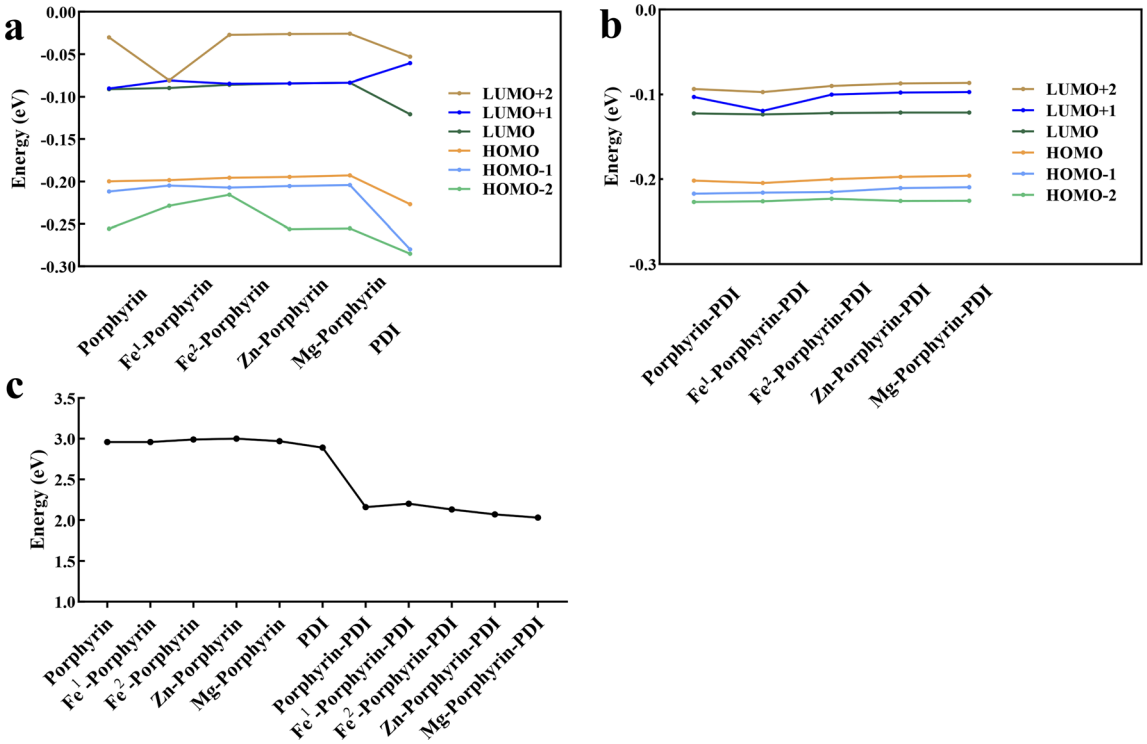

Fig. 3 Calculated frontier molecular orbital energies of ground states of (a) M-porphyrin and (b) M-porphyrin-PDI. (c) LUMO–HOMO energy gap.

time of charge relaxation and charge transfer between two molecules, AEA was chosen to calculate. The region around the Zn atom was analysed, as it is the most probable site for electron loss, with a calculated value of 47.37 kcal mol^{-1} (2.05 eV) during the adsorption of $^3O_2$ at a distance of 2.38 Å. Before adsorption, the overall average energies of Zn-porphyrin-PDI and $^3O_2$ were 0.20 kcal mol^{-1} (0.009 eV) and 1.02 kcal mol^{-1} (0.044 eV), respectively. After adsorption, these values shifted to 0.16 kcal mol^{-1} (0.007 eV) and −31.44 kcal mol^{-1} (−1.36 eV), respectively. These results are used to verify our point of view. In order to verify whether the designed PS molecules could pass electrons to $^3O_2$ to form O_2^- (type I), AEA values between $^3O_2$ and PS molecules were compared (Fig. 5). An ideal PS' AEA value should be less than that of $^3O_2$ to allow for the efficient transfer of electrons from the PS to oxygen, facilitating the reduction of oxygen.

$$\text{AEA}(^3O_2) - \text{AEA (PS)} > 0 \quad (3)$$

The calculated AEA of $^3O_2$ was 3.73 eV, hence porphyrin-PDI, Fe^2-porphyrin-PDI, Zn-porphyrin-PDI and Mg-porphyrin-PDI were screened as the possible candidates for PS that followed type I PDT mechanism.

3.4 Triplet excited states

To induce irreversible destruction of neoplastic tissues, the prevailing belief is that type II mechanisms should predominate in PDT, owing to their relatively higher reactivity.[48] To investigate the ability of the designed PS to excite $^3O_2$ to $^1O_2$, we compared the S_0–T_1 energy gap with the energy required to excite oxygen from $^3O_2$ to $^1O_2$.

$$\text{PS}(T_1) + {}^3O_2 \rightarrow \text{PS}(S_0) + {}^1O_2 \quad (4)$$

The energy needed for the formation of singlet oxygen is 0.98 eV.[44] The calculated data suggested that the value of S_0–T_1 energy gap was greater than 0.98 eV including porphyrin-PDI, Fe^2-porphyrin-PDI (Fig. 6). It was considered that these PS molecules designed here meet this energy requirement except the Fe^1-porphyrin and Fe^1-porphyrin-PDI, mainly due to their non-singlet ground state and possible multi spin state characteristics. The calculated S_1–T_1 energy gaps (ΔE_{ST}), provided in the ESI,† indicate that all compounds possess sufficient triplet state lifetimes, increasing their chances of reacting with oxygen to generate ROS. Except for Fe^1-porphyrin, the incorporation of PDI led to a slight reduction in the ΔE_{ST} across the compounds, suggesting that the presence of PDI enhances ISC efficiency by reducing the ΔE_{ST}.

3.5 Spin–orbit coupling matrix elements

In the process of ISC, the excited PS undergoes a transition from a singlet state to a triplet state. This triplet PS can then transfer its excitation energy to $^3O_2$, facilitating the generation of ROS. The efficiency of the ISC hinges on the amplitudes of SOC for the $S_1 \rightarrow T_n$ which effects the production of $^3O_2$.[49]

The value of SOC should be greater than 0.24 cm^{-1}. The SOC of the S_1–T_n (T_1–T_5) was calculated to discuss whether porphyrin

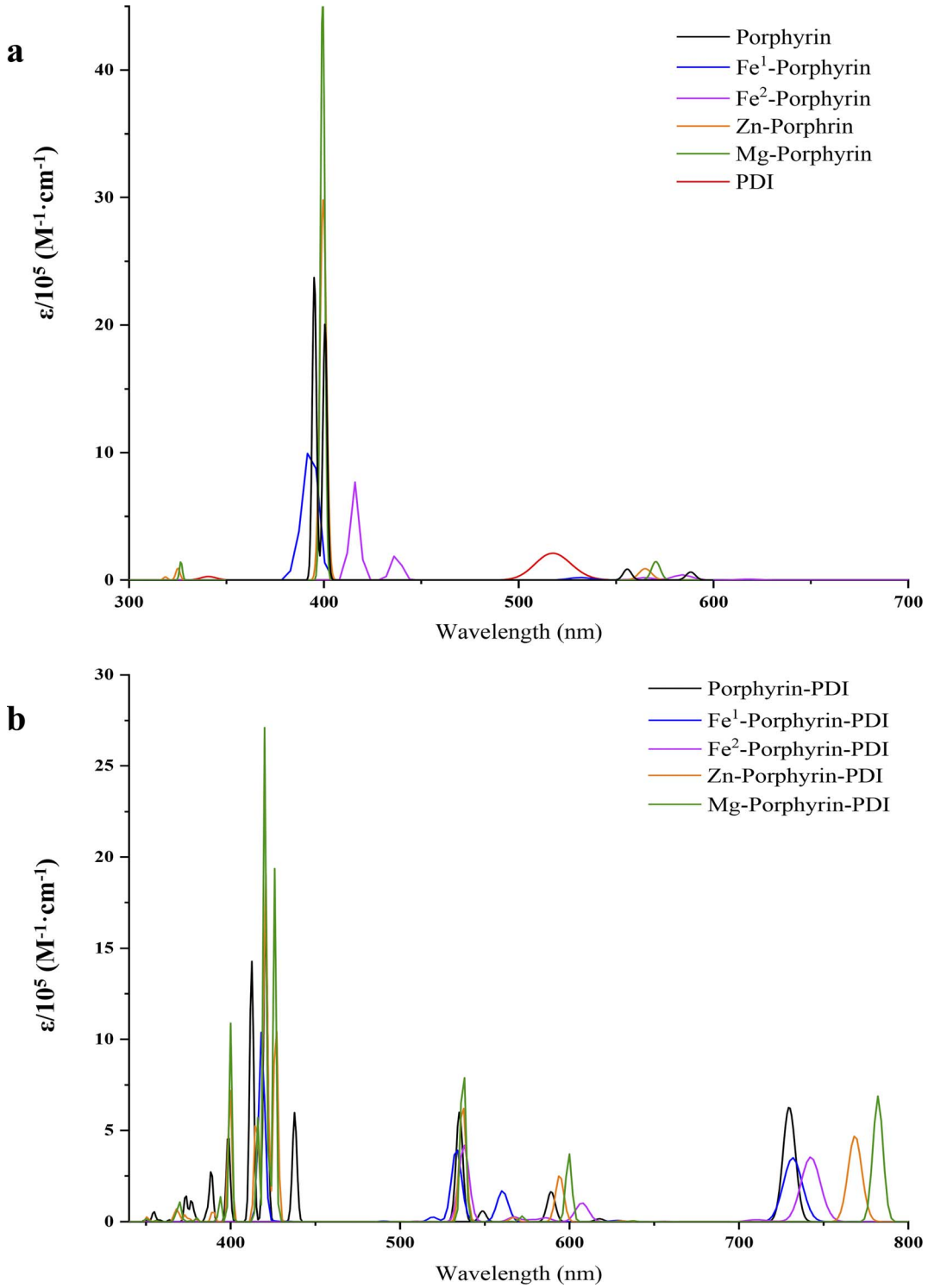

Fig. 4 Simulated absorption spectra of (a) M-porphyrin and (b) M-porphyrin-PDI.

complexes could have the effective coupling channel from S_1 to T_n (Fig. 7). Group 2 were met the requirements with 3–5 effective ISC channels. Comparing the SOC values for all the derivatives, it was observed that the insertion of PDI contributed to the enhancement of SOC's values.

A deficiency was found through the analysis of the above data. In the calculation of triplet excited states, Zn-porphyrin-PDI (0.94 eV) and Mg-porphyrin-PDI (0.97 eV) were applicable in the type I of PDT but did not playing a role in the type II of PDT. The structure of Zn-porphyrin-PDI, performing less in type II mechanism, was selected for improvement. Based on the

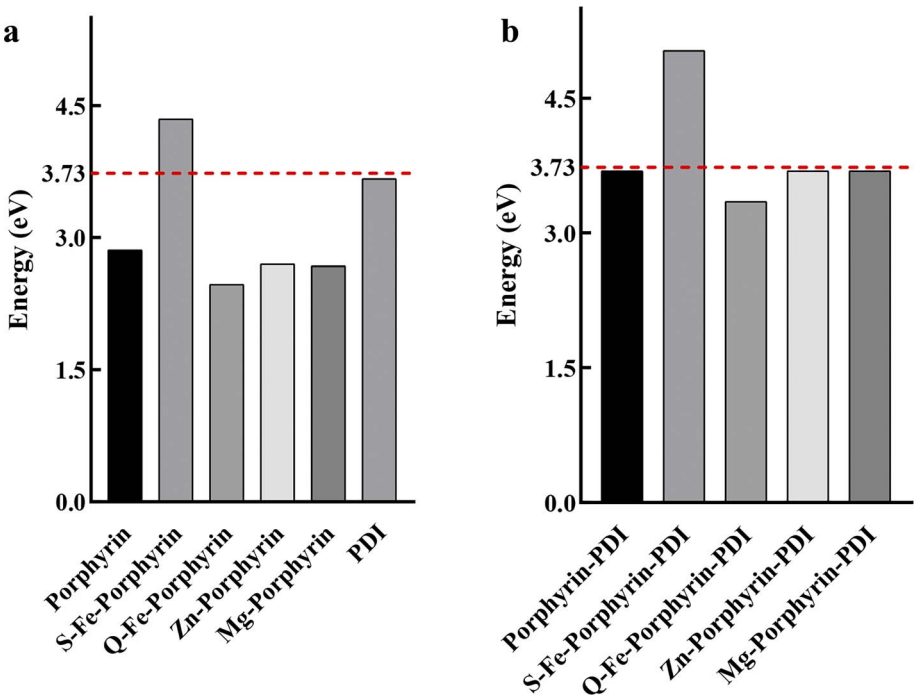

Fig. 5 Adiabatic electron affinities for (a) M-porphyrin and (b) M-porphyrin-PDI. The energy line of 3.73 eV for molecular oxygen was highlighted as the red dashed line.

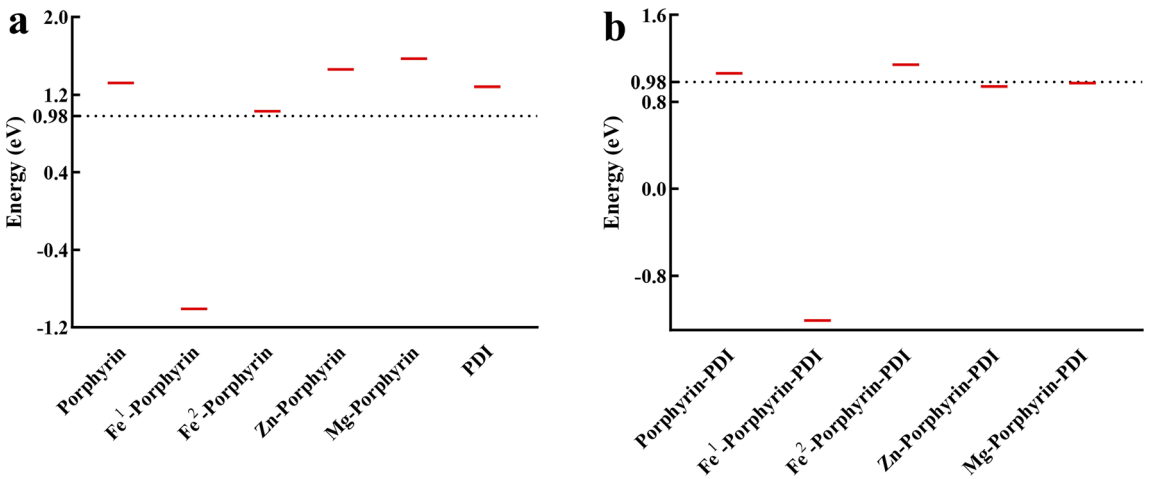

Fig. 6 Triplet excitation energies for (a) M-porphyrin and (b) M-porphyrin-PDI. The energy line of 0.98 eV, required to activate molecular oxygen, was highlighted as the black dashed line.

experience accumulated from the above work, the molecular configurations of Zn-porphyrin-PDI were expanded in group 3 by changing conjugate length and connective positions between Zn-porphyrin and PDI, or increasing the number of PDI on the basis of the Zn-porphyrin. We aimed to investigate how these structural modifications could enhance the PS's ability to generate ROS through both mechanisms. This approach was designed to better identify photosensitizers that can fulfill the requirements of both Type I and Type II mechanisms in PDT. Zn-porphyrin combined with PDI through single bond (compound **1**) or two acetylenic bonds (compound **2**). One PDI was added to Zn-porphyrin-PDI (compound **3**). Zn-porphyrin combined with the imide position of PDI by one acetylenic bond (compound **4**) or two acetylenic bonds (compound **5**) (Scheme 2). It was further screened based on previous calculation contents in group 3.

3.6 The calculations of Zn-porphyrin-PDI derivatives

The geometrically optimized structures of group 3 were shown in Fig. 8a. The frontier molecular orbitals were shown in Fig. 8b.

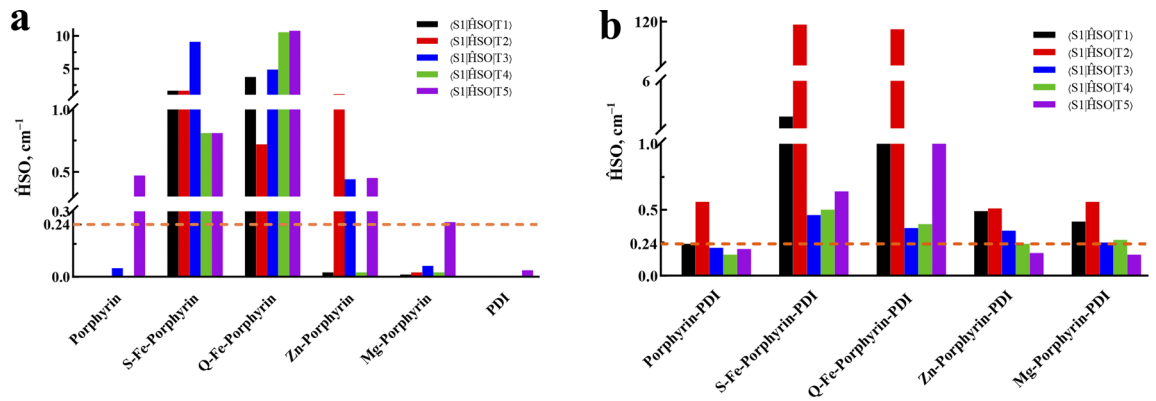

Fig. 7 Spin–orbit coupling matrix elements between low-lying singlet and triplet excited states for (a) M-porphyrin and (b) M-porphyrin-PDI.

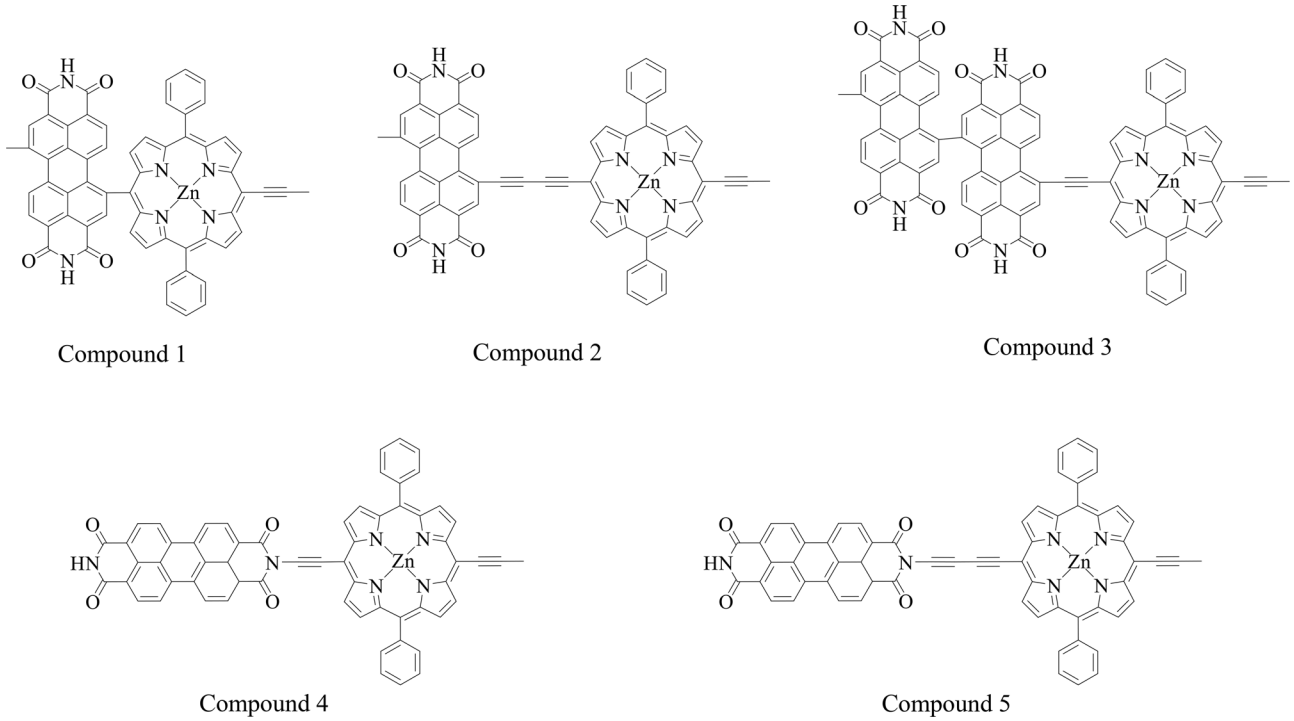

Scheme 2 Molecular structures of compound **1–5**.

The LUMO and HOMO were mainly located on the PDI derivatives and the porphyrin like Zn-porphyrin-PDI, respectively. The photophysical properties together with their orbital contribution were reported in Table 3. The results of the absorption spectra, frontier molecular orbitals, AEA, triplet excited states and SOC were demonstrated in Fig. 9. In the calculation of absorption spectra, the wavelengths of compound **1–3** were in phototherapy window (700–850 nm). Compared with Zn-porphyrin-PDI, decreasing conjugate length (compound **1**) would make absorption spectrum red-shift to 780.17 nm, and LUMO–HOMO gap and the triplet excited states energy grow to 2.14 eV and 1.34 eV, while AEA value decreased to 3.63 eV. Expending conjugate length (compound **2**) would blue-shift the wavelength to 750.48 nm, reducing LUMO–HOMO gap to 2.06 eV, while the AEA value and triplet excited states energy were increased to 3.84 eV and 1.31 eV, respectively. Adding an extra PDI to Zn-porphyrin-PDI (compound **3**) would red-shifted the absorption to 771.62 nm, shorten gap value and triplet excited states energy to 1.47 eV and 0.13 eV, and rise AEA value to 4.39 eV. After combining Zn-porphyrin with PDI's imide position (compound **4**), absorption peak blue-shifted to 606.40 nm. The gap value decreased to 1.95 eV. AEA value and triplet excited states energy up to 3.77 eV and 1.26 eV. Compared with compound **4**, extending conjugate length on the basis of the compound **4** (compound **5**) would red-shift the absorption peak value to 613.78 nm. Gap value, AEA value and the triplet excited states energy would increase to 2.02 eV, 3.78 eV and 1.36 eV. The ΔE_{ST} of M-porphyrin and M-porphyrin-

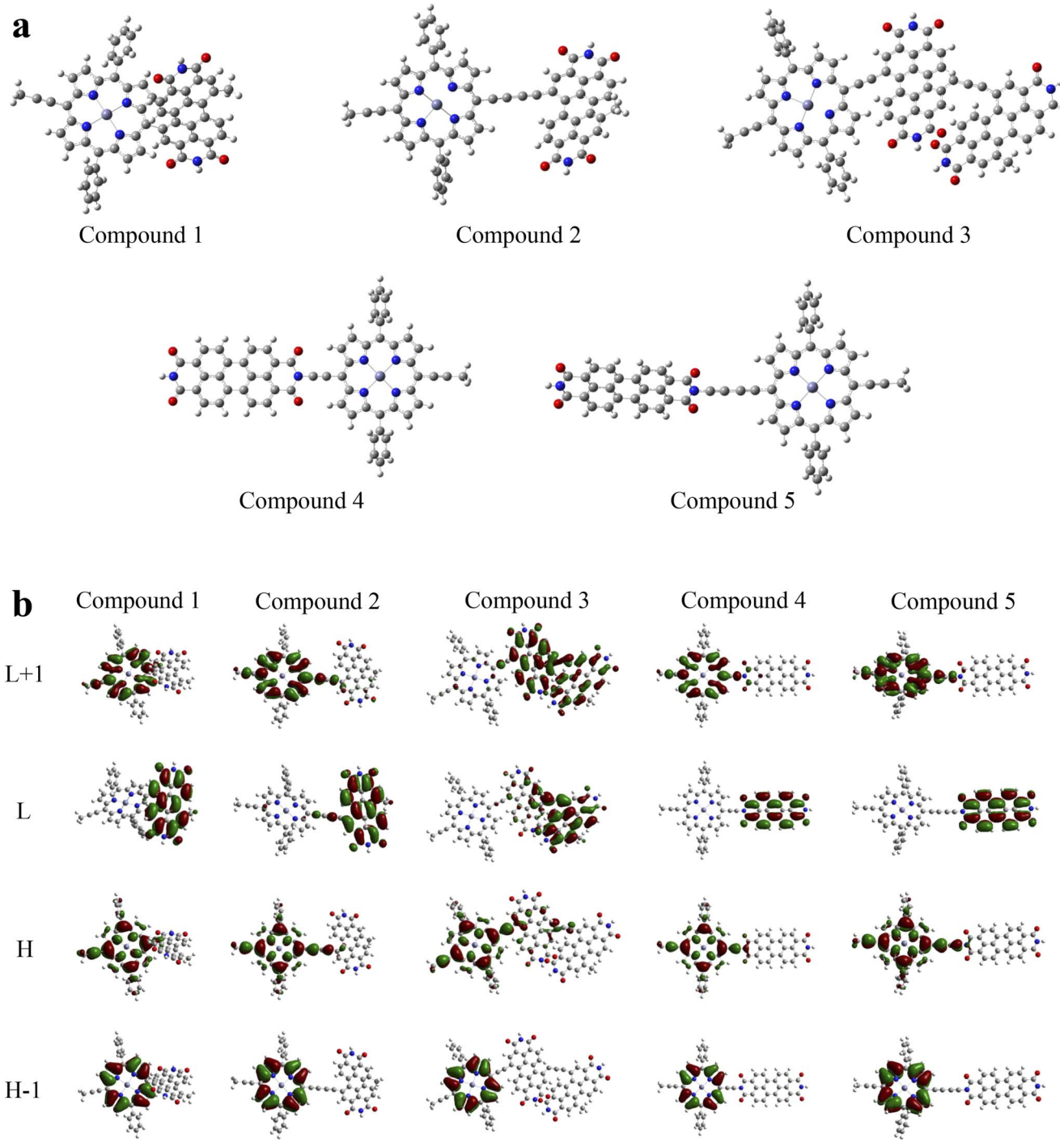

Fig. 8 (a) Optimized ground-state structures of compounds **1–5** and (b) illustrations of the molecular orbitals of compounds **1–5**.

Table 3 The essential vertical excitations of compound **1–5**

	Excitation energy (eV)	Wavelength (nm)	*f*	Main configuration
Compound **1**	1.5892	780.17	0.0807	H → L (99%)
Compound **2**	1.6521	750.48	0.3624	H → L (97%)
Compound **3**	1.6068	771.62	0.4452	H → L+1 (84%)
Compound **4**	2.0446	606.40	0.6136	H → L+1 (78%)
Compound **5**	2.0200	613.78	0.6529	H → L+1 (80%)

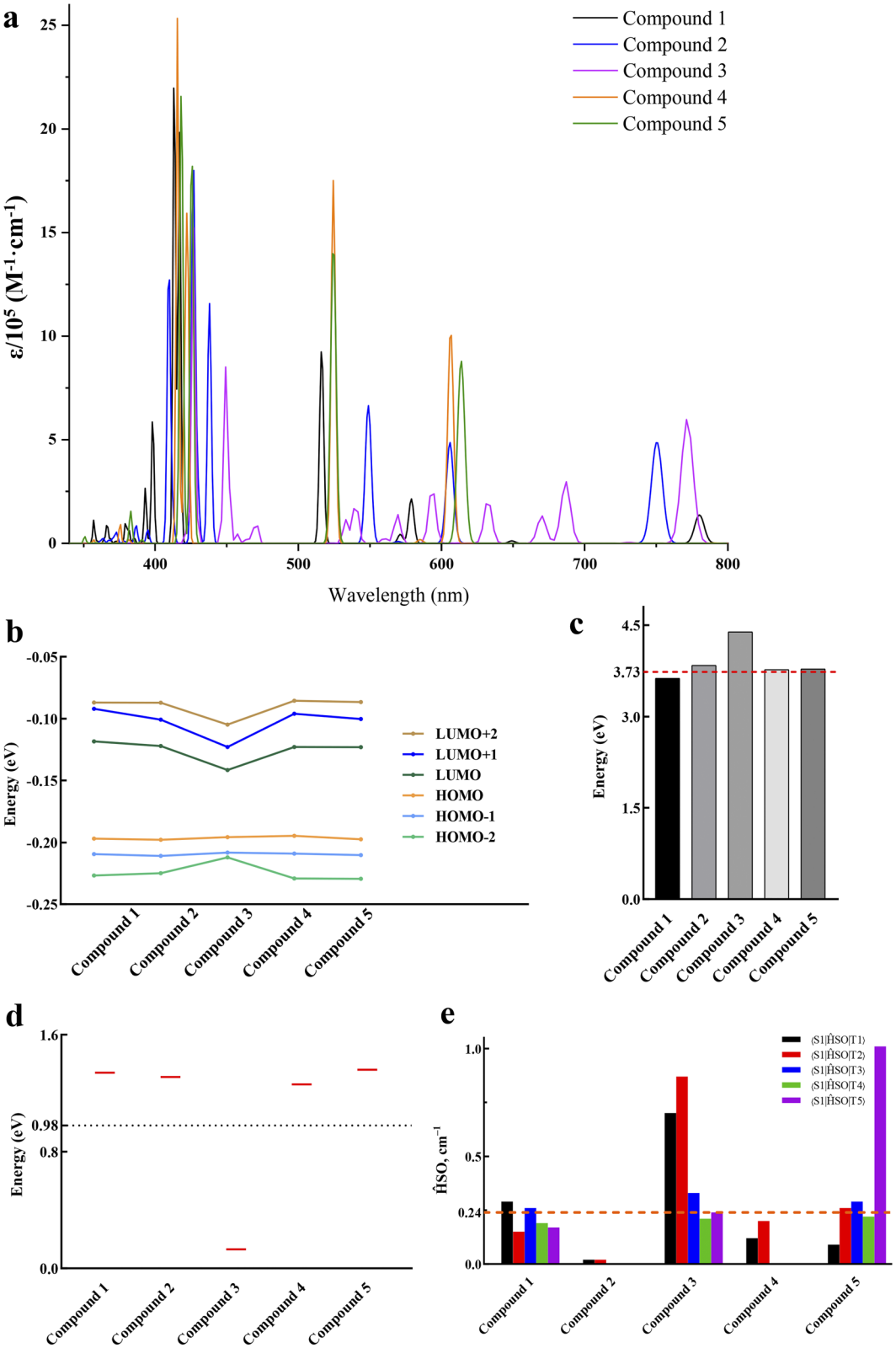

Fig. 9 (a) Calculated absorption spectra, (b) frontier molecular orbital energies, (c) adiabatic electron affinities, (d) triplet excitation energies and (e) spin–orbit coupling matrix elements of compound **1–5**.

PDI are provided in Table S2 (ESI†). Compared to Zn-porphyrin-PDI, increasing the number of PDI units does not significantly alter the ΔE_{ST}. However, modifying the conjugation length between the porphyrin and PDI or changing the substitution position on PDI can notably reduce the ΔE_{ST}, thereby enhancing ISC efficiency.

Table 4 Free energy of binding of selected compounds targeting Fas and Fasl

	Binding energy (kcal mol^{-1})	
Ligand	Fas	Fasl
Porphyrin-PDI	−9.8	−11.0
Fe^2-porphyrin-PDI	−10.2	−11.6
Zn-porphyrin-PDI	−10.4	−11.6
Mg-porphyrin-PDI	−10.3	−11.7
Compound **1**	−10.0	−9.7
Compound **2**	−10.1	−11.7

The results showed that the shorter the conjugate distance, the longer absorption wavelength, the lower AEA value would be. By combining with imide position of PDI could narrow LUMO–HOMO gap and increase the triplet excited states energy. However, gap value was decreased by adding an PDI. These allosteric strategies may also be applied to Mg-porphyrin derivatives based on the similar electronic structures and coordination condition of Mg-porphyrin and Zn-porphyrin derivatives. Therefore, compound **1** and **2** were screened as the possible candidates in group 3 that followed type I/II and type II PDT mechanism.

3.7 Molecular docking

Based on the above calculation results, we selected PS candidates applying the type I (porphyrin-PDI, Fe^2-porphyrin-PDI, Zn-porphyrin-PDI, Mg-porphyrin-PDI and compound **1**) and type II (porphyrin-PDI, Fe^2-porphyrin-PDI, compound **1** and **2**) mechanism for molecular docking study. The molecular docking is

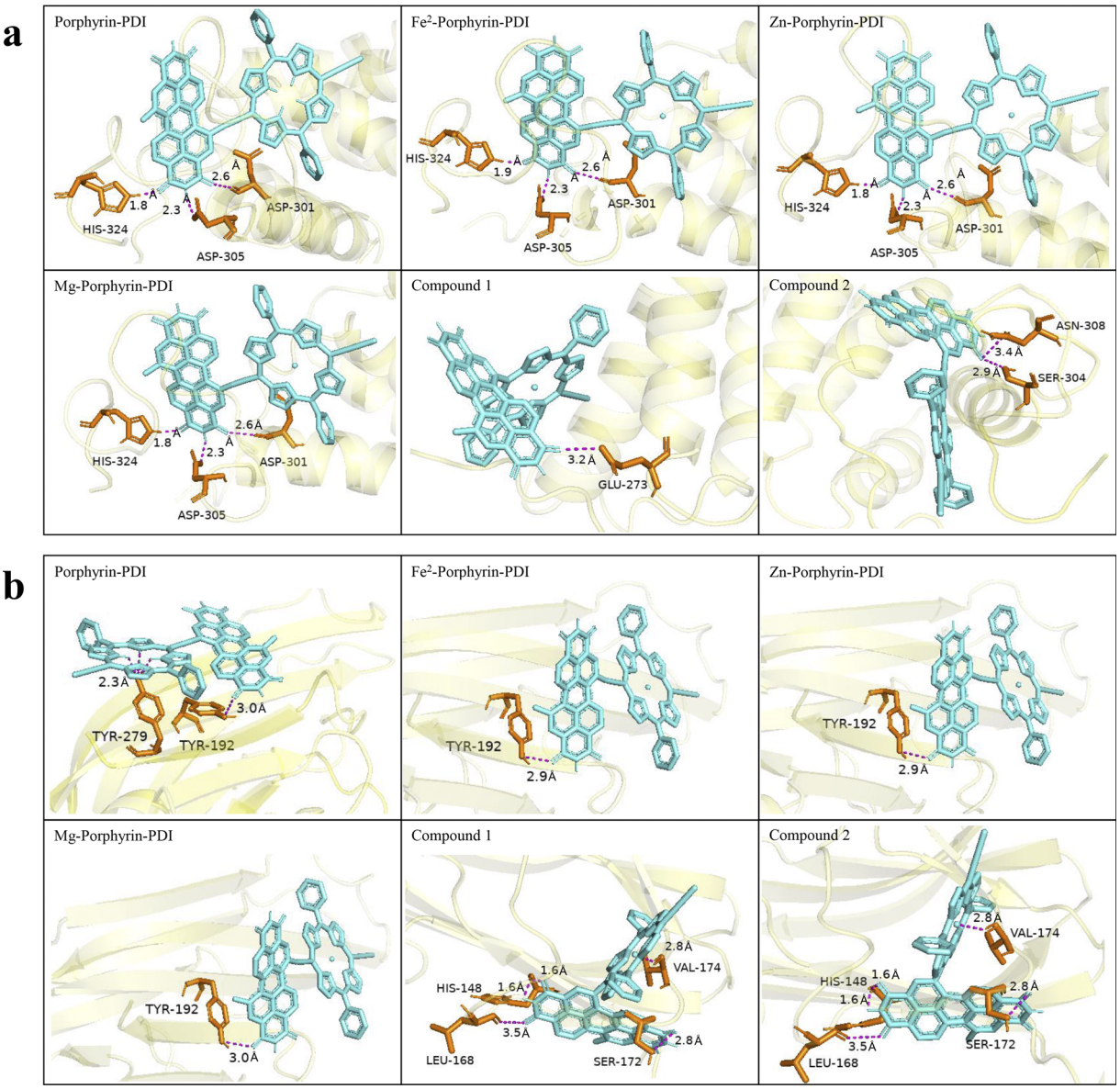

Fig. 10 Lowest energy docked positions of the PS candidates with cancer associated targeted proteins (a) Fas and (b) Fasl. The amino acid residues in the targeted proteins were shown by orange labels. Hydrogen bond interactions were represented in pink dashed lines and the corresponding hydrogen bond length values were marked.

an important method to clarify the interaction between a ligand and a target protein, which has been widely used for the structure-based drug design in pharmaceutical research.[50,51] In our study, the screened PS candidates, porphyrin-PDI, Fe^2-porphyrin-PDI, Zn-porphyrin-PDI, Mg-porphyrin-PDI, compound **1** and compound **2** were used as ligands. Fas and Fasl, apoptosis associated proteins, was one of the most important signal pathways of PDT research. At present, it has been verified that Aminolevulinate and chlorin e6 (they all belong to porphyrin precursors or porphyrins) can induce significantly greater Fas/Fasl which could further induce tumor cell apoptosis.[52,53] Thus, they were used as targeted proteins which were docked with the six selected PS candidates. The estimated free energy of binding (EFEB) (kcal mol^{-1}) values of the protein-ligand complexes were calculated. The EFEB of candidates which targeted Fas and Fasl were presented in Table 4.

The minimum energy docked positions and corresponding binding sites of the protein-ligand complexes were shown in Fig. 10. Meanwhile, the pink dashed lines indicated the hydrogen bonds formation between the ligand and selected targeted proteins. As can be observed from the figure, since the PDI portion possesses flexible and extended structural characteristics, the docking site initially emerges around the PDI and the final interaction is also mostly around the PDI fragment. The corresponding hydrogen bond length values between ligand molecules and the amino acid residues in the targeted proteins were also depicted in Fig. 10.

Previous research has demonstrated that metal ion coordination can modify the electronic structure and reactivity of molecules, leading to changes in energy. Additionally, metal coordination can strengthen interactions with specific regions of proteins.[54] Our results suggest that the incorporation of metals enhances the affinity between ligands and target proteins. However, the effect is relatively minor because the metal contributes to only one active site within the molecular framework, while the overall binding energy is influenced by the entire molecular structure. However, generally, more negative EFEB value was correlated with stronger binding affinity. A molecule has a good interaction with the proteins studied given by the values of EFEB lower than -6 kcal mol^{-1}.[55] All the candidates exhibited better binding capacity (from -9.8 to -11.7 kcal mol^{-1}). These effects are generally within the realm of weak interactions, and their impacts on the spectrum are similar to those of polar solvents. These minor effects do not alter our previous judgment of being good PDT candidates. The obtained results would be significative *in vitro* and *in vivo* studies for the development of effective PS in PDT.

Finally, at the same computational level, we conducted calculations for Foscan, which is utilized in the treatment of head and neck squamous cell carcinoma. The calculated values for AEA and T_1 were 2.88 eV and 1.56 eV, respectively. The S_1–T_n ($n = 1$–5) values for spin–orbit coupling were 0.05, 0, 0.01, 0, and 0.34 cm^{-1}, respectively. The EFEB of Fas and Fasl were -7.9 kal mol^{-1} and -7.4 kal mol^{-1}, respectively. In contrast, our screened PS candidates exhibited a distinct advantage in their ability to achieve a stable T_1 state and target the Fas/Fasl signaling pathway. Moreover, the porphyrin-based candidates are easily synthesized, with both porphyrin and PDI having verified feasible synthesis pathways.[56–58] Although their solubility as materials is not optimal, as small-molecule PS, they are still effective at inducing the PDT process even at extremely very low concentrations.[59–61] This is also the advantage of trace medication in PDT. Hence, porphyrinyl PS still possesses broad application prospects.

4 Conclusions

In summary, the conjugated porphyrin-based derivates with D–A structure were designed in this work using porphyrin without or with metals as electron donor and PDI as electron acceptor unit. Group 2 of metalloporphyrin-PDI and compound **1–3** of Zn-porphyrin-PDI PSs displayed intense absorbance in the NIR (700–850 nm) medical scope. Porphyrin-PDI, Fe^2-porphyrin-PDI, Zn-porphyrin-PDI, Mg-porphyrin-PDI and compound **1** could transfer electrons to perilesional molecular oxygen to produce ROS *via* type I mechanism of PDT efficiently. According to type II mechanism, porphyrin-PDI, Fe^2-porphyrin-PDI, compound **1** and **2** could excite $^3O_2$ to form $^1O_2$. All above screened candidates could also target Fas/Fasl signal pathway. Hence, the present investigations would be beneficial for the development of PS in PDT. For PDT process, in-depth understanding of the electronic state change behavior of the system induced by light excitation needs to be obtained at the chemical level in order to obtain the most effective key pharmacal efficacy information, so it is an essential research method for the development of such medicines. We believe that label extraction and machine learning based on this is an effective path for future typical pharmacologic development, and our following work is ongoing.

Data availability

All data generated or analysed during this study are included in this article.

Author contributions

Conceptualization, Fu-Quan Bai and Xin Liu; data curation, Wei-Huang Yin, Peng-Yuan Li, Hou-Hou Huang, Lu Feng and Shu-Hui Liu; funding acquisition, Fu-Quan Bai and Xin Liu; validation, Wei-Huang Yin; writing – original draft, Wei-Huang Yin and Peng-Yuan Li; writing – review & editing, Fu-Quan Bai.

Conflicts of interest

There are no conflicts to declare.

Acknowledgements

The present study was supported by a fund from Department of Science and Technology of Jilin Province, China (Grant No. 3D5203974430 & 3D5198153430) and the '14th Five-Year' Science and Technology Project of the Education Department of

Jilin province (Grant No. JJKH20220966KJ) and open fund of the state key laboratory of luminescent materials and devices of South China University of Technology, China (Grant No. 2022-skllmd-09).

Notes and references

1 M. A. Zaimy, N. Saffarzadeh, A. Mohammadi, H. Pourghadamyari, P. Izadi, A. Sarli, L. K. Moghaddam, S. R. Paschepari, H. Azizi, S. Torkamandi and J. Tavakkoly-Bazzaz, New methods in the diagnosis of cancer and gene therapy of cancer based on nanoparticles Cancer Gene Therapy, *Cancer Gene Ther.*, 2017, **24**, 233.

2 J. H. Correia, J. A. Rodrigues, S. Pimenta, T. Dong and Z. Yang, Photodynamic Therapy Review: Principles, Photosensitizers, Applications, and Future Directions, *Pharmaceutics*, 2021, **13**, 1332.

3 T. C. Pham, V. N. Nguyen, Y. Choi, S. Lee and J. Yoon, Recent Strategies to Develop Innovative Photosensitizers for Enhanced Photodynamic Therapy, *Chem. Rev.*, 2021, **121**, 13454–13619.

4 L. Larue, B. Myrzakhmetov, A. Ben-Mihoub, A. Moussaron, N. Thomas, P. Arnoux, F. Baros, R. Vanderesse, S. Acherar and C. Frochot, Fighting Hypoxia to Improve PDT, *Pharmaceuticals*, 2019, **12**, 163.

5 W. Domka, D. Bartusik-Aebisher, W. Mytych, K. Dynarowicz and D. Aebisher, The Use of Photodynamic Therapy for Head, Neck, and Brain Diseases, *Int. J. Mol. Sci.*, 2023, **24**, 11867.

6 X. Li, J. F. Lovell, J. Yoon and X. Chen, Clinical development and potential of photothermal and photodynamic therapies for cancer, *Nat. Rev. Clin. Oncol.*, 2020, **17**, 657–674.

7 P. Sarbadhikary, B. P. George and H. Abrahamse, Recent Advances in Photosensitizers as Multifunctional Theranostic Agents for Imaging-Guided Photodynamic Therapy of Cancer, *Theranostics*, 2021, **11**, 9054–9088.

8 R. Alzeibak, T. A. Mishchenko, N. Y. Shilyagina, I. V. Balalaeva, M. V. Vedunova and D. V. Krysko, Targeting immunogenic cancer cell death by photodynamic therapy: past, present and future, *J. Immunother. Cancer*, 2021, **9**, 001926.

9 J. A. Rodrigues and J. H. Correia, Photodynamic Therapy for Colorectal Cancer: An Update and a Look to the Future, *Int. J. Mol. Sci.*, 2023, **24**, 12204.

10 L. G. Arellano, E. M. Villar-Alvarez, B. Velasco, V. Domínguez-Arca, G. Prieto, A. Cambón, S. Barbosa and P. Taboada, Light excitation of gold Nanorod-Based hybrid nanoplatforms for simultaneous bimodal phototherapy, *J. Mol. Liq.*, 2023, **377**, 121511.

11 J. Wang, Z. Cao, P. Wang, X. Zhang, J. Tang, Y. He, Z. Huang, X. Mao, S. Shi and X. Kou, Apoptotic Extracellular Vesicles Ameliorate Multiple Myeloma by Restoring Fas-Mediated Apoptosis, *ACS Nano*, 2021, **15**, 14360–14372.

12 J. Zhu, P.-F. Petit and B. J. Van den Eynde, Apoptosis of tumor-infiltrating T lymphocytes: a new immune checkpoint mechanism, *Cancer Immunol. Immunother.*, 2018, **68**, 835–847.

13 P. Agostinis, K. Berg, K. A. Cengel, T. H. Foster, A. W. Girotti, S. O. Gollnick, S. M. Hahn, M. R. Hamblin, A. Juzeniene, D. Kessel, M. Korbelik, J. Moan, P. Mroz, D. Nowis, J. Piette, B. C. Wilson and J. Golab, Photodynamic therapy of cancer: an update, *Ca-Cancer J. Clin.*, 2011, **61**, 250–281.

14 G. Gunaydin, M. E. Gedik and S. Ayan, Photodynamic Therapy-Current Limitations and Novel Approaches, *Front. Chem.*, 2021, **9**, 691697.

15 C. Donohoe, M. O. Senge, L. G. Arnaut and L. C. Gomes-da-Silva, Cell death in photodynamic therapy: from oxidative stress to anti-tumor immunity, *Biochim. Biophys. Acta Rev. Canc*, 2019, **1872**, 188308.

16 X. Wang, H. Lv, Y. Sun, G. Zu, X. Zhang, Y. Song, F. Zhao and J. Wang, New porphyrin photosensitizers-Synthesis, singlet oxygen yield, photophysical properties and application in PDT, *Spectrochim. Acta, Part A*, 2022, **279**, 121447.

17 X. Jiang, Y. Zhao, S. Sun, Y. Xiang, J. Yan, J. Wang and R. Pei, Research development of porphyrin-based metal-organic frameworks: targeting modalities and cancer therapeutic applications, *J. Mater. Chem. B*, 2023, **11**, 6172–6200.

18 J. B. C. Dhiman Maitra, J. S. Elenbaas, H. L. Bonkovsky, J. A. Shavit and M. Bishr Omary, Porphyrin-Induced Protein Oxidation and Aggregation as a Mechanism of Porphyria-Associated Cell Injury, *Cell. Mol. Gastroenterol. Hepatol.*, 2019, **8**, 536–548.

19 N. Tsolekile, S. Nelana and O. S. Oluwafemi, Porphyrin as Diagnostic and Therapeutic Agent, *Molecules*, 2019, **24**, 2669.

20 M. Lan, S. Zhao, W. Liu, C. S. Lee, W. Zhang and P. Wang, Photosensitizers for Photodynamic Therapy, *Adv. Healthc. Mater.*, 2019, **8**, e1900132.

21 J. Ke, X. Zhao, J. Yang, K. Ke, Y. Wang, M. Yang and W. Yang, Enhanced Ion-Selective Diffusion Achieved by Supramolecular Interaction for High Thermovoltage and Thermal Stability, *Energy Environ. Mater.*, 2023, **7**, e12562.

22 X. Wei, W. b. Cui, G.-y. Qin, X. e. Zhang, F. y. Sun, H. Li, J. f. Guo and A. m. Ren, Theoretical Investigation of Ru(II) Complexes with Long Lifetime and a Large Two-Photon Absorption Cross-Section in Photodynamic Therapy, *J. Med. Chem.*, 2023, **66**, 4167–4178.

23 Z. Zhao, N. Xu, Y. Wang, G. Ling and P. Zhang, Perylene diimide-based treatment and diagnosis of diseases, *J. Mater. Chem. B*, 2021, **9**, 8937–8950.

24 H. Li, L. Yue, M. Wu and F. Wu, Self-assembly of methylene violet-conjugated perylene diimide with photodynamic/photothermal properties for DNA photocleavage and cancer treatment, *Colloids Surf. B Biointerfaces*, 2020, **196**, 111351.

25 H. Lu, J. Liu, Y. Liu, X. Xu and Z. Bo, Improving the Efficiency of Organic Solar Cells by Introducing Perylene Diimide Derivative as Third Component and Individually Dissolving Donor/Acceptor, *ChemSusChem*, 2021, **14**, 5442–5449.

26 X. Wu, H. Wang, Y. Gong, D. Fan, P. Ding, Q. Li and Q. Qian, Graph neural networks for molecular and materials representation, *J. Mater. Inf.*, 2023, **3**, 12.

27 X. Pan, J. Wu, L. Xiao, B. Yap, R. Xia and X. Peng, Porphyrin Acceptors with Two Perylene Diimide Dimers for Organic Solar Cells, *ChemSusChem*, 2021, **14**, 3614–3621.

28 F. Yang, Y. Wu, J. Zhao, Y. Guo, X. Guo, W. Li and J. Wang, Excited-state photophysical processes in a molecular system containing perylene bisimide and zinc porphyrin chromophores, *Phys. Chem. Chem. Phys.*, 2020, **22**, 20891–20900.

29 C. Li, Z. Luo, L. Yang, J. Chen, K. Cheng, Y. Xue, G. Liu, X. Luo and F. Wu, Self-assembled porphyrin polymer nanoparticles with NIR-II emission and highly efficient photothermal performance in cancer therapy, *Mater. Today. Bio*, 2022, **13**, 100198.

30 R. A. Timothy, H. Louis, E. A. Adindu, T. E. Gber, E. C. Agwamba, O. E. Offiong and A. M. S. Pembere, Elucidation of collagen amino acid interactions with metals (B, Ni) encapsulated graphene/PEDOT material: insight from DFT calculations and MD simulation, *J. Mol. Liq.*, 2023, **390**, 122950.

31 H. Nakashima, J. Y. Hasegawa and H. Nakatsuji, On the O2 binding of Fe-porphyrin, Fe-porphycene, and Fe-corrphycene complexes, *J. Comput. Chem.*, 2006, **27**, 1363–1372.

32 M. Walker, A. J. Harvey, A. Sen and C. E. Dessent, Performance of M06, M06-2X, and M06-HF density functionals for conformationally flexible anionic clusters: M06 functionals perform better than B3LYP for a model system with dispersion and ionic hydrogen-bonding interactions, *J. Phys. Chem. A*, 2013, **117**, 12590–12600.

33 P. R. c. á. Thomas Malcomson, S. Erhardt and M. J. Paterson, Protocols for Understanding the Redox Behavior of Copper Containing Systems, *ACS Omega*, 2022, **7**, 45057–45066.

34 W. J. Hehre, R. Ditchfield and J. A. Pople, Self-Consistent Molecular Orbital Methods. XII. Further Extensions of Gaussian-Type Basis Sets for Use in Molecular Orbital Studies of Organic Molecules, *J. Chem. Phys.*, 1972, **56**, 2257–2261.

35 P. J. Hay and W. R. Wadt, Ab initio effective core potentials for molecular calculations. Potentials for K to Au including the outermost core orbitals, *J. Chem. Phys.*, 1985, **82**, 299–310.

36 S. Grimme, J. Antony, S. Ehrlich and H. Krieg, A consistent and accurate ab initio parametrization of density functional dispersion correction (DFT-D) for the 94 elements H-Pu, *J. Chem. Phys.*, 2010, **132**, 154104.

37 M. J. Frisch, G. W. Trucks, H. B. Schlegel, G. E. Scuseria, M. A. Robb, J. R. Cheeseman, G. Scalmani, V. Barone, G. A. Petersson, H. Nakatsuji, X. Li, M. Caricato, A. V. Marenich, J. Bloino, B. G. Janesko, R. Gomperts, B. Mennucci, H. P. Hratchian, J. V. Ortiz, A. F. Izmaylov, J. L. Sonnenberg, W. F. Ding, F. Lipparini, F. Egidi, J. Goings, B. Peng, A. Petrone, T. Henderson, D. Ranasinghe, V. G. Zakrzewski, J. Gao, N. Rega, G. Zheng, W. Liang, M. Hada, M. Ehara, K. Toyota, R. Fukuda, J. Hasegawa, M. Ishida, T. Nakajima, Y. Honda, O. Kitao, H. Nakai, T. Vreven, K. Throssell, J. A. Montgomery Jr, J. E. Peralta, F. Ogliaro, M. J. Bearpark, J. J. Heyd, E. N. Brothers, K. N. Kudin, V. N. Staroverov, T. A. Keith, R. Kobayashi, J. Normand, K. Raghavachari, A. P. Rendell, J. C. Burant, S. S. Iyengar, J. Tomasi, M. Cossi, J. M. Millam, M. Klene, C. Adamo, R. Cammi, J. W. Ochterski, R. L. Martin, K. Morokuma, O. Farkas, J. B. Foresman and D. J. Fox, *Gaussian 16 (Revision B.01)*, Wallingford CT, Gaussian Inc., 2016.

38 J. D. Chai and M. Head-Gordon, Long-range corrected hybrid density functionals with damped atom-atom dispersion corrections, *Phys. Chem. Chem. Phys.*, 2008, **10**, 6615–6620.

39 F. Neese, F. Wennmohs, U. Becker and C. Riplinger, The ORCA quantum chemistry program package, *J. Chem. Phys.*, 2020, **152**, 224108.

40 G. M. Morris, R. Huey and A. J. Olson, Using AutoDock for Ligand-Receptor Docking, *Current protocols in bioinformatics*, 2008, ch. 8, pp. 8–14.

41 *The PyMOL Molecular Graphics System, Version 2.0*, Schrödinger, LLC.

42 L. Ulfo, P. E. Costantini, M. Di Giosia, A. Danielli and M. Calvaresi, EGFR-Targeted Photodynamic Therapy, *Pharmaceutics*, 2022, **14**, 241.

43 A. V. Soldatova, J. Kim, C. Rizzoli, M. E. Kenney, M. A. Rodgers, A. Rosa and G. Ricciardi, Near-infrared-emitting phthalocyanines. A combined experimental and density functional theory study of the structural, optical, and photophysical properties of Pd(II) and Pt(II) alpha-butoxyphthalocyanines, *Inorg. Chem.*, 2011, **50**, 1135–1149.

44 A. Drzewiecka-Matuszek and D. Rutkowska-Zbik, Application of TD-DFT Theory to Studying Porphyrinoid-Based Photosensitizers for Photodynamic Therapy: A Review, *Molecules*, 2021, **26**, 7176.

45 X. Wang, F. Q. Bai, Y. Liu, Y. Wang, H. X. Zhang and Z. Lin, A Computational Way To Achieve More Effective Candidates for Photodynamic Therapy, *J. Chem. Inf. Model.*, 2017, **57**, 1089–1100.

46 L. Noriega, M. E. Castro, J. M. Perez-Aguilar, N. A. Caballero, B. L. Sanchez-Gaytan, E. Gonzalez-Vergara and F. J. Melendez, Oxidovanadium(V) complexes as promising anticancer photosensitizers, *J. Inorg. Biochem.*, 2020, **203**, 110862.

47 G. P. Zu, J. J. Wang, Y. Zhang, W. B. Chen, Y. Z. Shi, S. W. Guo and X. R. Wang, Study on Five Porphyrin-Based Photosensitizers for Singlet Oxygen Generation, *ChemistrySelect*, 2019, **4**, 863–867.

48 B. C. De Simone, M. E. Alberto, N. Russo and M. Toscano, Photophysical properties of heavy atom containing tetrasulfonyl phthalocyanines as possible photosensitizers in photodynamic therapy, *J. Comput. Chem.*, 2021, **42**, 1803–1808.

49 M. Spiegel and C. Adamo, Tuning the Photophysical Properties of Ru(II) Photosensitizers for PDT by Protonation and Metallation: A DFT Study, *J. Phys. Chem. A*, 2023, **127**, 3625–3635.

50 T. Valarmathi, R. Premkumar, M. R. Meera and A. Milton, Franklin Benial, Spectroscopic, quantum chemical and molecular docking studies on 1-amino-5-chloroanthraquinone: A targeted drug therapy for thyroid cancer, *Spectrochim. Acta Mol. Biomol. Spectrosc.*, 2021, **255**, 119659.

51 L. G. Ferreira, R. N. Dos Santos, G. Oliva and A. D. Andricopulo, Molecular docking and structure-based drug design strategies, *Molecules*, 2015, **20**, 13384–13421.
52 K. A. Salva, Y. H. Kim, Z. Rahbar and G. S. Wood, Epigenetically Enhanced PDT Induces Significantly Higher Levels of Multiple Extrinsic Pathway Apoptotic Factors than Standard PDT, Resulting in Greater Extrinsic and Overall Apoptosis of Cutaneous T-cell Lymphoma, *Photochem. Photobiol.*, 2018, **94**, 1058–1065.
53 L. Zhao, X. Rao, R. Zheng, C. Huang, R. Kong, X. Yu, H. Cheng and S. Li, Targeting glutamine metabolism with photodynamic immunotherapy for metastatic tumor eradication, *J. Controlled Release*, 2023, **357**, 460–471.
54 C. Abbehausen, Zinc finger domains as therapeutic targets for metal-based compounds-an update, *Metallomics*, 2019, **11**, 15–28.
55 A. M. Udrea, A. Dinache, A. Staicu and S. Avram, Target Prediction of 5,10,15,20-Tetrakis(4'-Sulfonatophenyl)-Porphyrin Using Molecular Docking, *Pharmaceutics*, 2022, **14**, 2930.
56 F. R. L. A. D. Adler, J. D. Finarelli, J. Goldmacher, J. Assour and L. Korsakoff, A simplified synthesis for meso-tetraphenylporphine, *J. Org. Chem.*, 1967, **32**, 476.
57 J. S. Lindsey, I. C. Schreiman, H. C. Hsu, P. C. Kearney and A. M. Marguerettaz, Rothemund and adler-longo reactions revisited synthesis of tetraphenylporphyrins under equilibrium, *J. Org. Chem.*, 1987, **52**, 827–836.
58 A. Nowak-Król and F. Würthner, Progress in the synthesis of perylene bisimide dyes, *Org. Chem. Front.*, 2019, **6**, 1272–1318.
59 I. Yakavets, M. Millard, V. Zorin, H.-P. Lassalle and L. Bezdetnaya, Current state of the nanoscale delivery systems for temoporfin-based photodynamic therapy: advanced delivery strategies, *J. Controlled Release*, 2019, **304**, 268–287.
60 F. Espitia-Almeida, C. Diaz-Uribe, W. Vallejo, D. Gomez-Camargo, A. R. R. Bohorquez, X. Zarate and E. Schott, Photophysical characterization and in vitro anti-leishmanial effect of 5,10,15,20-tetrakis(4-fluorophenyl) porphyrin and the metal (Zn(II), Sn(IV), Mn(III) and V(IV)) derivatives, *BioMetals*, 2022, **35**, 159–171.
61 L. Zhang, Y. Geng, L. Li, X. Tong, S. Liu, X. Liu, Z. Su, Z. Xie, D. Zhu and M. R. Bryce, Rational design of iridium-porphyrin conjugates for novel synergistic photodynamic and photothermal therapy anticancer agents, *Chem. Sci.*, 2021, **12**, 5918–5925.